

Modulational instability and quantum droplets in a two-dimensional Bose-Einstein condensate

Sherzod R. Otajonov, Eduard N. Tsoy, and Fatkhulla Kh. Abdullaev

Physical-Technical Institute of the Uzbek Academy of Sciences,

Chingiz Aytmatov Str. 2-B, Tashkent, 100084, Uzbekistan

Abstract

Modulational instability of a uniform two-dimensional binary Bose-Einstein condensate (BEC) in the presence of quantum fluctuations is studied. The analysis is based on the coupled Gross-Pitaevskii equations. It is shown that quantum fluctuations can induce instability when the BEC density is below a threshold. The dependence of the growth rate of modulations on the BEC parameters is found. It is observed that an asymmetry of the interaction parameters and/or initial densities of the components typically decreases the growth rate. Further development of the instability results in a break-up of the BEC into a set of quantum droplets. These droplets merge dynamically with each other so that the total number of droplets decreases rapidly. The rate of this decrease is evaluated numerically for different initial parameters.

I. INTRODUCTION

Modulation instability (MI), or the Benjamin-Fair instability [1, 2], is a well-known phenomenon in physics. The main effect of MI is an exponential growth of the modulation amplitude of a plane wave. MI has been studied in different fields of physics, such as nonlinear optics, plasma physics, hydrodynamics, and the physics of Bose-Einstein condensates (BECs), see e.g. [3–5]. A usual method for studying MI in BECs is based on the linear stability analysis of a stationary plane-wave. The dynamics of MI in the presence of additional effects has been considered in many works. These works include a study of MI of matter-waves under a strong periodic variation in time of the scattering length [6], MI in chiral BECs with zero-energy nonlinearity [7], and the influence of three-body interaction on MI in coupled nonlinear systems [8]. A nonlinear stage of the MI has also been studied [9, 10].

According to the mean-field theory, MI in single-component BECs occurs only for the attractive two-body atomic interaction. This is because the attractive interaction counteracts a condensate expansion caused by the quantum pressure. The presence of MI in two-component BECs depends on the relationship between the values of the parameters of interactions [11, 12]. For example, the attractive inter-component interaction might induce MI, even when both components have the self-repulsive interaction. When both intra- and inter-species interactions are repulsive, MI can still occur due to the development of out-of-phase structures in the components [12].

A study of MI is important because the instability is a precursor to the formation of spatially localized patterns, such as bright solitons and self-bound quantum droplets (QDs). Recent theoretical studies of 1D binary BEC have been reported in Refs. [13] where MI results in the formation of multiple QDs.

A quantum droplet is a structure with a localized distribution of the condensate density. In contrast to bright solitons that can have an arbitrary peak density, the peak density of QDs is limited. The peak density of a condensate in QDs is small for a small number of atoms, and it saturates at a large number of atoms [14–19]. Therefore, the properties of QDs with a large number of atoms are similar to those of incompressible liquids. A possibility of a formation of QDs in BECs due to quantum fluctuations were predicted theoretically in Refs. [14, 15].

The effect of quantum fluctuations is small compared with the two-body interaction. Both the quantum fluctuation parameter and the two-body interaction parameter depend on the scattering length, and therefore they cannot be varied independently via the Feshbach resonance. Quantum fluctuations can be made noticeable by using, for example, two-component or dipolar condensates. In these systems, one can tune the parameters of atomic interactions independently of the strength of quantum fluctuations. In a binary BEC, parameters of the interaction between atoms can be chosen such that there is a small residual attraction. This attraction can result in a collapse of a BEC. However, quantum fluctuations that introduce a repulsion can prevent collapse. In dipolar BECs, the strength of the dipolar interaction and the scattering length can be tuned independently, such that the effect of quantum fluctuations becomes perceptible.

The static and dynamical properties of QDs in 1D without external confinement are investigated theoretically in Refs. [16, 17]. Exact solutions, collisions of QDs, and the period of oscillations of a breathing mode are found. Two different regimes of QDs depending on the QD size or the number of atoms are also identified. In the 2D case, stability regions of QDs with embedded vorticity are found numerically in Ref. [18]. For analytical treatment of 2D QDs and vortices, the variational approximation is proposed in Ref. [19]. In 3D, properties of two-component QDs and vortices are reported in Ref. [20], stability regions are found for vortices $S=1$ and 2, where S is the topological charge. The dynamics of QDs under the periodic variation of scattering parameters is studied in Ref. [21]. Collective oscillations of the Lee-Huang-Yang fluid are investigated in Ref. [22].

The existence of QDs has been confirmed experimentally in different physical systems, such as single-component BECs with dipole-dipole interaction [23, 24], homonuclear [25, 26], and heteronuclear [27] bosonic mixtures. These theoretical and experimental studies have opened new perspectives for the investigation of fundamental properties of quantum gases under the action of quantum fluctuations [28, 29].

We consider in this work a system with a contact interaction and quantum fluctuations. The present study aims to investigate the linear and nonlinear stages of MI, and the formation of QDs in a binary 2D BEC. The structure of the paper is as follows. In Sec. II A we introduce the model equations for the description of a binary 2D BEC. The linear stability analysis is presented in Sec. II B. Stability/instability regions are found for different values of the parameters. The nonlinear stage of MI is analyzed in Sec. II C. The number of emerging

QDs is estimated, and its variation in time is analyzed using image processing methods. In Sec. III we summarize our findings.

II. THE MODEL AND RESULTS

A. The model

In Ref. [15], the energy density of two-dimensional binary BECs in the presence of quantum fluctuations is derived. Also, the Gross-Pitaevskii equation is obtained via a standard variation of the energy density functional. In 2D, the contribution of quantum fluctuations depends logarithmically on the condensate density, and this is the specific property of atomic scattering in two dimensions. The dynamics of a two-component BEC under the action of quantum fluctuations is described by the coupled Gross-Pitaevskii equations [15], see also [18, 19]:

$$i\hbar \frac{\partial \Psi_j}{\partial T} + \frac{\hbar^2}{2m} \nabla^2 \Psi_j - \frac{g_j m}{4\pi \hbar^2} P_j \log \left[\frac{em}{\hbar^2 \Delta} P \right] \Psi_j - \sqrt{g_j} (\sqrt{g_j} |\Psi_j|^2 - \sqrt{g_{3-j}} |\Psi_{3-j}|^2) \Psi_j = 0, \quad (1)$$

where Ψ_j is a wave function of the component, $j = 1$ and 2 , $\nabla^2 = \partial_x^2 + \partial_y^2$ is the two-dimensional Laplacian, T is the time, m is the atomic mass, $P = g_1 |\Psi_1|^2 + g_2 |\Psi_2|^2$, $g_j = 4\pi \hbar^2 \sigma_j / m$ is the intra-species interaction parameter, $\sigma_j = 1 / \log[4e^{-2\gamma} / a_j^2 \Delta]$, $\Delta = \frac{4e^{-2\gamma}}{a_{12} \sqrt{a_1 a_2}} \exp \left[\frac{-\log^2(a_2/a_1)}{2 \log[a_{12}^2 / (a_1 a_2)]} \right]$, parameters a_1, a_2 and a_{12} are the 2D scattering lengths, and e and γ are the Euler number and the Euler constant, respectively. Following Ref. [15], we consider the case of the weak intra-species repulsion ($g_1, g_2 > 0$) and inter-species attraction ($g_{12} < 0$). The parameter g_{12} is taken such that $g_{12}^2 = g_1 g_2$, this relation is reflected in the definition of parameter Δ . Equation (1) shows that when the interaction parameters (g_1, g_2, g_{12}) tend to zero, the effect of quantum fluctuations ($\sim g^2$) is negligible. By a proper choice of the interaction parameters and the component densities, it is possible to make the strength of quantum fluctuations [the third term in Eq. (1)] comparable with the two-body interaction [the last term in Eq. (1)]. Also, notice that quantum fluctuations in 2D result in a self-attraction for small P (the re-scaled density) and a self-repulsion for large P [15].

By using new variables, $\psi = \Psi/\psi_s$, $t = T/t_s$ and $(x, y) = (X, Y)/r_s$, where scale parameters ψ_s , t_s and r_s are defined as:

$$\begin{aligned} \psi_s &= (\Delta/8\pi e\sqrt{\sigma_1\sigma_2})^{1/2}, & t_s &= me/\hbar\Delta\sqrt{\sigma_1\sigma_2}, \\ r_s &= (e/\Delta\sqrt{\sigma_1\sigma_2})^{1/2}, \end{aligned} \quad (2)$$

Eq. (1) is reduced to the following dimensionless form:

$$\begin{aligned} i \frac{\partial \psi_j}{\partial t} + \frac{1}{2} \nabla^2 \psi_j - \frac{\psi_j}{2\sqrt{\sigma_1\sigma_2}} \left(\sqrt{\sigma_j/\sigma_{3-j}} |\psi_j|^2 - |\psi_{3-j}|^2 \right) - \\ \sqrt{\sigma_j/\sigma_{3-j}} \psi_j p \log(p) = 0, \end{aligned} \quad (3)$$

where $\nabla^2 = \partial_x^2 + \partial_y^2$ and $p = (\sigma_1|\psi_1|^2 + \sigma_2|\psi_2|^2)/(2\sqrt{\sigma_1\sigma_2})$. All theoretical and numerical results are for the dimensionless equation. However, in Sec. II C we also provide parameters in physical units. A uniform distribution of the condensate is described by a plane wave solution of Eq. (3):

$$\psi_j = A_j \exp(-i \mu_j t), \quad (4)$$

where A_j and μ_j are the amplitude and chemical potential of the j -th component, respectively. The dependence of the chemical potentials on the amplitudes is found from Eq. (3) and (4):

$$\mu_j = \frac{A_j^2}{2\sigma_{3-j}} - \frac{A_{3-j}^2}{2\sqrt{\sigma_j\sigma_{3-j}}} + \sqrt{\sigma_j/\sigma_{3-j}} p \log(p). \quad (5)$$

In the following Sections, we study the growth of modulations of the uniform state (Sec. II A B), and the formation of QDs in the later stage of instability (Sec. II A C).

B. The linear stage of MI

For the linear stability analysis, we study the dynamics of small perturbations $\delta\psi_j \ll A_j$ imposed on the stationary state

$$\psi_j = (A_j + \delta\psi_j) \exp(-i \mu_j t). \quad (6)$$

The small-amplitude dynamics of $\delta\psi_j$ is described by the following equations:

$$\begin{aligned} i \frac{\partial \delta\psi_j}{\partial t} + \frac{1}{2} (\delta\psi_{jxx} + \delta\psi_{jyy}) - c_j (\delta\psi_j^* + \delta\psi_j) - \\ c_3 (\delta\psi_{3-j}^* + \delta\psi_{3-j}) = 0, \end{aligned} \quad (7)$$

where $j = 1$ and 2 ,

$$c_j \equiv \frac{A_j^2}{2\sigma_{3-j}} + \frac{A_j^2\sigma_j}{2\sigma_{3-j}} \log(ep_0), \quad (8)$$

$$c_3 \equiv \frac{A_1 A_2}{2} \left[-\frac{1}{\sqrt{\sigma_1 \sigma_2}} + \log(ep_0) \right], \quad (9)$$

and $p_0 = (\sigma_1 A_1^2 + \sigma_2 A_2^2)/(2\sqrt{\sigma_1 \sigma_2})$.

We represent the perturbation as $\delta\psi_j = u_j + i v_j$, and split Eq. (7) into the real and imaginary parts. Assuming that $(u_j, v_j) \sim \exp(\lambda t + i k_x x + i k_y y)$ we get the following characteristic equation:

$$\begin{aligned} \lambda^4 + \lambda^2 k^2 \left(c_1 + c_2 + \frac{k^2}{2} \right) + \frac{k^8}{16} + \\ \frac{k^6}{4} (c_1 + c_2) + k^4 (c_1 c_2 - c_3^2) = 0, \end{aligned} \quad (10)$$

where $k^2 = k_x^2 + k_y^2$.

Equation (10) is a bi-quadratic equation on λ , and its solution is

$$\lambda_{\pm}^2 = \frac{k^2}{4} \left[-k^2 - 2(c_1 + c_2) \pm 2\sqrt{(c_1 - c_2)^2 + 4c_3^2} \right]. \quad (11)$$

A plane wave is modulationally unstable if the following conditions are fulfilled:

$$ep_0 < 1, \quad \text{and} \quad |k| < k_{cr}, \quad (12)$$

where the critical value k_{cr} is defined as:

$$|k| < k_{cr} \equiv \sqrt{2} \sqrt{-(c_1 + c_2) + \sqrt{(c_1 - c_2)^2 + 4c_3^2}}. \quad (13)$$

For $\sigma_1 = \sigma_2$, parameter p_0 is equal $n_0/2$. Therefore, condition (12) states that MI occur at sufficiently low densities. The real part of exponents, $G \equiv \text{Re}(\lambda_{\pm}) > 0$, characterizes the growth rate of MI. If $ep_0 > 1$, the system is modulationally stable. When $ep_0 = 1$, terms with logarithm, associated with a contribution from quantum fluctuations, in Eqs. (8) and (9) become zero. We recall that the presence of MI in a binary system without quantum fluctuations depends on relative values of intra- and inter-species interaction parameters [12]. For our choice of g_1 , g_2 and g_{12} , the system without quantum fluctuations is neutrally stable. This means that the growth rate is zero for these parameters, and the system is modulationally stable. Quantum fluctuations induce a self-attraction for low densities.

This can result in the emergence of MI and QDs in the system. We mention that QDs in binary BECs have been observed experimentally in Refs. [25–27], where the role of quantum fluctuations was revealed.

The maximum value of the MI growth rate G_{max} is attained at the corresponding $k = k_{max}$, where

$$G_{max} = \frac{k_{max}^2}{2} = \frac{k_{cr}^2}{4}, \quad k_{max} = \frac{k_{cr}}{\sqrt{2}}. \quad (14)$$

In the symmetric case, $\sigma_1 = \sigma_2 = \sigma$ and $A_1 = A_2 = A$, equations for MI parameters G and k_{cr} are simplified, because $c_1 = c_2 = A^2[1/\sigma + \log(eA^2)]/2$ and $c_3 = A^2[-1/\sigma + \log(eA^2)]/2$. We analyze the dynamics for different sets of parameters. In all cases studied, it is found that for a given total density $n_0 = n_{10} + n_{20} \equiv A_1^2 + A_2^2$, parameter G_{max} is larger for the symmetric case, compared with asymmetric cases. In particular, when the density of one component is small, the corresponding c_j and c_3 are also small. Then, k_{cr} is negligible, assuming $c_1, c_2 > 0$, so MI exists in a narrow region of k , with the low growth rate, see Eq. (14).

In Fig. 1(a), the MI growth rate as a function of the modulation wave number k is plotted for the symmetric (a top line) and the asymmetric (a bottom line) cases. The growth rate profile has a typical (half-) butterfly shape. Points in Fig. 1(a) show the results of numerical simulations. The dependence of G on k and n_0 for the symmetric case is presented in Fig. 1(b). One can see that MI exists only if the BEC total density is sufficiently small. This is due to the repulsive nature of quantum fluctuations at large densities. We mention that MI and the formation of chains of QDs in 1D binary BEC were analyzed theoretically in Ref. [13].

An influence of asymmetry of the BEC parameters on the MI growth rate is shown in Fig. 2. The rate G as a function of initial amplitudes (n_{10}, n_{20}) for given $\sigma_1 = \sigma_2 = 0.1$ is shown in Fig. 2(a). The instability region is below $n_{20} = 2/e - n_{10}$ line, see Eq. (12). Maximum of G , which equals to 0.135 for such values of σ_1 and σ_2 , is realized also for the symmetric case.

In Fig. 2(b), the instability region in (σ_1, σ_2) -plane is between two straight lines $\sigma_2 = \sigma_1 A_2^{-4}(-A_1^2 A_2^2 + 2/e^2 \pm (2/e)\sqrt{1/e^2 - A_1^2 A_2^2})$. Figure 2(b) is plotted for $n_{10} = n_{20} = 0.271$, a value that corresponds to the maximum gain 0.135 in Fig. 2(a). For a given $n_{10} = n_{20}$, the maximum value of the growth rate attains at the diagonal $\sigma_2 = \sigma_1$, and it does not depend on the values of σ_j on that line. We conclude from Fig. 2 that asymmetry of the

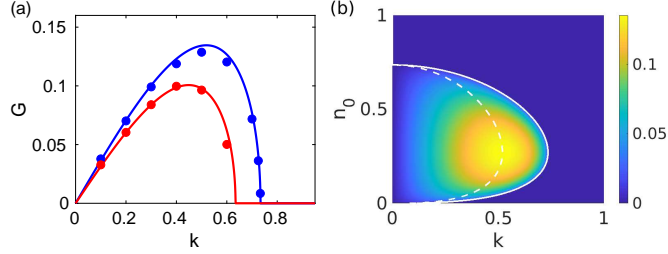


FIG. 1. (a): The MI growth rate G vs k . The top (blue) line for the symmetric case $n_{10} = n_{20} = 0.3$ and the bottom (red) line for the asymmetric case $n_{10} = 0.3$ and $n_{20} = 0.1$. Points are found from direct numerical simulations of Eq. (3). (b): The growth rate G as a function of k and n for the symmetric case. The solid line shows the MI boundary, see Eq. (13), and the dashed line represents G_{max} , see Eq. (14). The interaction parameters are $\sigma_1 = \sigma_2 = 0.1$.

system parameters and/or of the component densities results typically in a decrease of the MI growth rate.

Our analysis suggests the following way to observe MI in experiments. Firstly, one needs to create a high-density two-component condensate. For this condition, the condensate is stable. Then, a decrease of the density n , for example, by expanding an external trap, can induce MI when condition (12) is satisfied.

Due to the instability, the uniform state is transformed into a structure of peaks and dips. These peaks can be associated with strongly overlapped QDs. The distance between the peaks is $\sim 2\pi/k_{max}$. Therefore, the number of QDs per unit area is evaluated as $\rho_0 = K_0/L^2$, where $K_0 = k_{max}^2 L^2 / (2\pi)^2$ is the number of generated QDs. We mention that parameters K_0 and ρ_0 are valid for the linear stage of MI, when $t < t_{th}$. The threshold time t_{th} can be estimated as the time when the modulation amplitude is of order $\sim 0.1A_0$, $t_{th} \simeq G_{max}^{-1} \log(0.1A_0/\epsilon)$, where ϵ is the initial amplitude of modulations.

In order to check the dynamics, we perform numerical simulations of Eq. (3) in the domain $-50 \leq L(= L_x = L_y) \leq 50$, with 1024×1024 grid points. The size of the domain is much larger than the typical size of droplets, which emerged in the linear stage of MI ($L \gg 1/k_{max}$). We use the split-step Fourier transform method with periodic boundary conditions. We employ two types of initial conditions. The first type of initial conditions is a plane wave with periodic modulations $\delta\psi(x, y, 0) = \epsilon \cos(k_x x) \cos(k_y y)$. The second type is a plane wave with random modulations. In experiments, the instability is typically

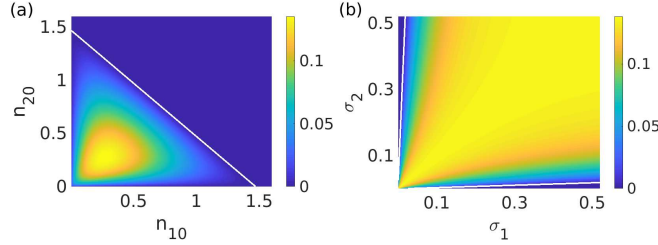


FIG. 2. (a) The growth rate of MI in (n_{10}, n_{20}) -plane for $\sigma_j = 0.1$. Maximum of the growth rate equals 0.135 at $n_{10} = n_{20} = 0.271$. (b) The growth rate in (σ_1, σ_2) -plane for $n_{10} = n_{20} = 0.271$. In both figures, lines represent the instability boundaries, see Eq. (13).

induced from random perturbations, consisting of modes in a wide range of k . All unstable k contribute to the growth of modulations. However, the wave mode with $k = k_{max}$ that corresponds to the maximum of gain dominates in the dynamics. We observe that by using random modulations, the dynamics do not depend strongly on initial conditions in different runs, see Sec.II C.

In order to obtain the growth rate for a particular k , we use periodic modulations with $\epsilon = 10^{-3}$. We monitor the dependence of the maximum modulation amplitudes on time and recover the value of the growth rate G . Points, found from numerical simulations of Eq. (3), in Fig. 1(a) match well with the prediction of the linear theory. We also mention that for regular perturbations with given k , the density distribution almost returns to its initial stage with very small modulations. This resembles a well-known MI recurrence phenomenon [30]. However, after 2-5 cycles of returning to the initial stage, an interaction between droplets occurs.

C. The nonlinear stage of MI

We use numerical simulations in order to analyse the development of MI. As an initial condition, we use a noisy plane wave $\psi_j(x, y, 0) = A_j[1 + \epsilon R(x, y)]$, where $\epsilon \ll 1$, and $R(x, y)$ is a random function with the uniform distribution of values in a range $(-1, 1)$.

Figures 3(a) and (b) show typical patterns of the overlapped droplets developed in the linear stage of MI. In Fig. 3(a), the density distribution still corresponds to a modulated plane wave with $n(x, y, t)$ near the initial value n_0 (notice a different scale on this subplot). This means that there is no fragmentation of the BEC into droplets in Fig. 3(a). Figure 3(b) shows

a result of a plane wave break-up into distinguishable QDs such that intervals between them have zero density. The mean numbers of generated QDs, found over several simulations, on this stage are in a qualitative agreement with the value K_0 , obtained from the linear analysis, see also Fig. 5. One can see that some QDs are located close to each other, forming continuous clusters. The distance between QDs is close to the size of droplets. Therefore there is a strong interaction between QDs that causes their merging.

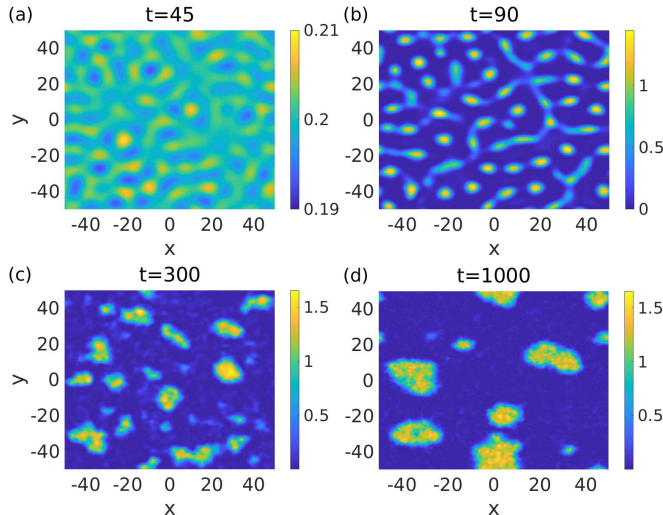


FIG. 3. The typical dynamics of the density distribution $n = |\psi_1|^2 + |\psi_2|^2$ at (a) $t = 45$, (b) $t = 90$, (c) $t = 300$, and (d) $t = 1000$. The initial densities are $n_0 = 0.2$, and $\sigma_1 = \sigma_2 = 0.1$.

A process of the merging results in the creation of larger QDs, as seen in Fig. 3(c) and (d). Since the shape of QDs is far from a stationary form, and due to the merging, there are strong oscillations of particle amplitudes and widths. Moreover, the density distribution within a single droplet is also non-uniform and varies on time. However, we do not observe a noticeable movement of QDs within the plane. We mention that a similar merging (coalescence) of droplets in a BEC with the cubic-quintic interaction was reported in Ref. [33].

We measure numerically the maximum $n_{max} \equiv \max_{x,y}[n(x,y,t)]$, the minimum $n_{min} \equiv \min_{x,y}[n(x,y,t)]$, and the average n_{av} of the BEC density, where $n(x,y,t) \equiv |\psi_1|^2 + |\psi_2|^2$, see Fig. 4(a). Parameter n_{av} is found within QDs, i.e. we exclude points where $n(x,y,t) < 0.5 n_{max}$. One can see that at $t \gtrsim 90$, the system is in the nonlinear stage. After a rapid increase, n_{max} varies near a constant value. This value corresponds to spikes of BEC density oscillations of different QDs. Average density n_{av} of QDs is well below n_{max} . This density

can be estimated from the following reasoning. As it is found in Ref. [18, 19], the peak density of quantum droplets saturates at a large number N_{QD} of particles within a single droplet. This fact reflects the liquid nature of QDs. As demonstrated in Ref. [19], the peak density of a stationary QD for the symmetric case can be found approximately from

$$n_{st} = 2 \exp\left(-\frac{1}{2} + \frac{1}{2m} - \frac{2^{1/m}\pi m}{N_{QD}}\right), \quad (15)$$

where the form parameter m is defined as $m = (0.4433 + 0.05906N_{QD})^{0.5047}$ for $N_{QD} = [1, 1000]$. Equation (15) is derived, assuming a super-Gaussian profile of a QD, i.e. $\psi(x, y, t) \sim \sqrt{n_{st}} \exp[-(r/w)^{2m}/2]$. Factor 2 in front of the exponent in Eq. (15), compared with the corresponding equation in Ref. [19], accounts for two components. Stationary amplitude n_{st} tends to the Thomas-Fermi limit [18] $n_{TF} = 2/\sqrt{e}$, when $N_{QD} \rightarrow \infty$. As it follows from Fig. 4(a), average density n_{av} indeed approaches on time to the Thomas-Fermi limit. During the development of MI, maximum droplet density n_{max} rises, while n_{min} vanishes. This corresponds to a break up of a plane wave into separated QDs (c.f. Fig. 3(a) and (b)).

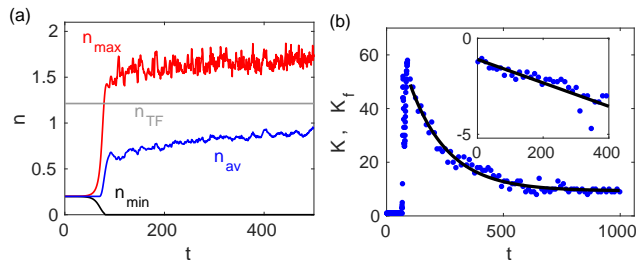


FIG. 4. (a) Time evolution of n_{max} (top line), and n_{min} (bottom line), n_{av} (middle line) for $n_0 = 0.2$, and $\sigma_1 = \sigma_2 = 0.1$. The straight line represents the Thomas-Fermi limit n_{TF} (b) The number K of generated QDs on time. Points are found from direct numerical simulations, the line is found from the exponential regression. The parameters of fitting are $a = 75.28$, $\beta = 0.0057$, $t_b \simeq 90$, $b = 8.57$. The inner plot shows this relation in logarithmic scale. The horizontal and vertical axis are $t - t_b$ and $\log[(K - b)/a]$, respectively.

As follows from Eq. (12), in the symmetric case, plane waves with $n_0 > 2/e$ are stable. At the same time, the peak density n_{st} of QDs is changed from 0 at $N_{QD} = 0$ to $n_{TF} = 2/\sqrt{e}$ at $N_{QD} \rightarrow \infty$. This suggests that QDs with large N_{QD} should be stable against small modulations, while those with small N_{QD} can be unstable. However, in Ref. [18, 19] it

was shown that QDs with an arbitrary number of particles are stable. We suppose that small-amplitude QDs are stable due to the quantum pressure.

When the initial densities are not equal, the scenario of the droplet formation is different. Let us consider, for example, the case $A_1 > A_2$. The density maxima $n_{max,1}$ and $n_{max,2}$ of the components are increased on time during the interaction of QDs, while the minima $n_{min,1}$ and $n_{min,2}$ are decreased, similarly to the case of equal initial amplitudes, c. f. Fig. 4. This process of the sharp variation ends when the density minimum $n_{min,2}$ reaches zero. After that, parameters $n_{max,1}$, $n_{max,2}$ and $n_{min,1}$ are changed gradually, with random fluctuations. In regions between droplets, the density of the first component $n_1(x, y) \sim n_{min,1}$, while $n_2(x, y) \sim 0$. However, emerged droplets consist of the condensate mixture. Therefore, at later stages, the density distribution corresponds to a set of two-component droplets immersed in a single-component background. This is similar to droplets of water in a cloud of vapor.

We recall the instability is suppressed in the absence of one component. Further development of MI on the background is ceased or is decelerated due to a negligible value of the density of the second component in regions between droplets. We mention that this type of dynamics is observed when the difference between the initial densities is appreciable (more than 10-20%). If the initial densities of the components are close to each other, the dynamics is similar to the symmetric case.

The number $K(t)$ of QDs is found from the density distribution analysis. Namely, we transform the density distribution $n(x, y, t)$ to a black-and-white image in (x, y) -plane, using $0.5 n_{max}(t)$ as a threshold, and we count the number of connected components (islands). We mention that a choice of a different threshold (e.g. $0.7 n_{max}$) does not change strongly the results obtained. For small times, $K(t)$ equals one, since at each point, $n(x, y, t) > 0.5 n_{max}(t)$. When instability is developed, $K(t)$ grows rapidly due to emergence of droplets from small modulations, see Fig. 4(b). We mention that this rapid increase can be non-monotonic, that is value $K(t)$ can oscillates and have local maxima during this growth. Starting from $t = t_b$, the number of QDs decreases exponentially. Therefore, time t_b corresponds to the boundary between the rapid growth and the decrease of the number of QDs. This decrease is due to merging of overlapped droplets. Points in Fig. 4(b) show a variation of $K(t)$ in a single run of numerical simulations, and the line represents the averaged fitting curve.

We fit the dependence $K(t)$, using the following function

$$K_f(t) = a \exp[-\beta (t - t_b)] + b, \quad t > t_b. \quad (16)$$

Parameter a , b and β , which is the decrement of the number of QDs, are independent fitting coefficients. For each realization of an initial condition, we obtain the fitting coefficients. These coefficients are averaged over ten runs. This averaged parameters are used for the fitting curve $K_f(t)$ in Fig. 4(b). The inner plot in Fig. 4(b), shown on a semi-logarithmic scale, justifies our choice of the fitting function.

We study numerically the dynamics of QDs also for different values of n_0 . In Fig. 5, a solid line shows the number ρ_0 , found from the MI analysis, of QDs per unit area versus the initial density n_0 . Points represent averaged values ρ_{av} of QDs per unit area, found from numerical simulations of Eq. (3) at $t = t_b$. Time t_b of the beginning of the exponential decrease of $K(t)$ is different in different realizations of initial conditions. In order to get t_b , we find average values of the number of droplets at each moment of time, obtaining $K_{av}(t)$. We choose the position of the global maximum of this dependence as time t_b , and we use this fixed value for obtaining (a, b, β) in different runs for a given n_0 . Then, in each run $K(t_b) = a + b$, so that $\rho_b = (a + b)/L^2$. The average of ρ_b over ten runs is presented in Fig. 5. The vertical error bars correspond to the standard deviation. A reasonable agreement of the theory of the linear regime and simulations justifies our approach of counting the QD number. Triangular points, connected with a dashed line, show the dependence of the average decrement β_{av} on n_0 .

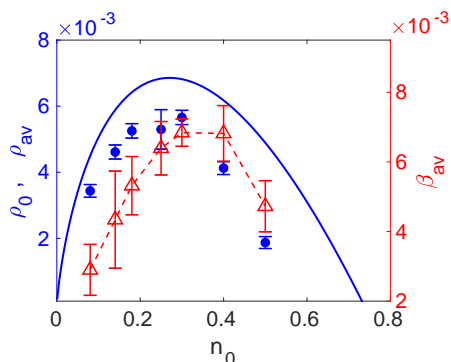


FIG. 5. The number of generated QDs per unit area ρ_0 (solid line), found from the MI theory, the averaged number ρ_{av} (circles), found from numerical simulations of Eq. (3), and the averaged decrement β_{av} of the QD number (triangles, right axes) vs the initial density n_0 .

For estimation of experimentally relevant parameters, we consider a BEC of ^{39}K atoms in different spin states. In dimensional reduction from 3D to 2D, there is a relation between two- and three-dimensional scattering lengths, $\vec{a}^{(2D)} = (4\pi/B)^{1/2}l_0 \exp(-\gamma - \sqrt{\pi/2}l_0/\vec{a}^{(3D)})$, where $B = 0.915$, $l_0 = (\hbar/m\omega_\perp)^{1/2}$ is the harmonic oscillator length, ω_\perp is the radial confinement frequency, see Ref. [15]. For both dimensions the vector \vec{a} has the following components (a_1, a_2, a_{12}) .

The 2D case is realized when the transverse confinement is sufficiently strong. For ^{39}K , such a confinement is achieved for frequency $\omega_\perp/2\pi \sim 10 - 50$ kHz that corresponds to the harmonic oscillator length $l_0 \sim (100 - 50)$ nm. We mention that the use of traps with such frequencies is reported in a number of works, see e.g. Ref. [31, 32]. Three-dimensional intra- and inter-species scattering length are taken as $a_1^{(3D)}$ and $a_2^{(3D)} \sim 500 a_0$, and $a_{12}^{(3D)} = -(0.9 - 0.99) a_1^{(3D)}$, where a_0 is the Bohr radius. The characteristic scales of the system are $r_s \sim (3 - 0.6) \mu\text{m}$, $t_s \sim (6 - 0.2)$ ms, $N_s \sim 10 - 2$. Values of parameter σ_j are found to be in the range $\sim (0.06 - 0.15)$. These parameters are achievable in experiments on BECs.

III. CONCLUSIONS

We have studied modulational instability in two-dimensional binary Bose-Einstein condensates under the action of quantum fluctuations. Modulational instability occurs only for low densities when $ep_0 < 1$, otherwise, the system is stable. Analytical equations for the spectrum of the MI growth rate have been obtained. Instability regions of perturbed plane waves in the parameter space have been found. The main peculiarity of MI in a system with quantum fluctuations is the existence of the threshold density above which the system is stable. It has been demonstrated by means of numerical simulations that the development of MI results in the formation of droplets. Interestingly, in the case of unequal initial densities of components, these droplets are separated by a non-zero background. From the analysis of the nonlinear stage of the MI, we have obtained the number $K(t)$ of generated QDs. It has been shown that the number of QDs decreases rapidly due to merging, and the decrease rate β of this number has been estimated. Theoretical predictions are corroborated by the numerical simulations of governing equations. Our work shows a practical application of an image processing technique for analyzing the BEC density distribution.

ACKNOWLEDGEMENTS

This work has been funded from the State budget of the Republic of Uzbekistan.

- [1] T. B. Benjamin and J. E. Feir, The disintegration of wave trains on deep water. 1. Theory, *J. Fluid Mech.* **27**, 417 (1967).
- [2] L. A. Ostrovskii, Propagation of wave packets and space-time self-focusing in a nonlinear medium, *Zh. Eksp. Teor. Fiz.* **51** 1189 (1966). *Transl. Sov. Phys. JETP.* **24**, 797 (1967).
- [3] G. P. Agrawal, *Nonlinear fiber optics* (Academic Press, 2019).
- [4] A. Hasegawa, *Plasma instability and nonlinear effects* (Springer-Verlag, Heidelberg, 1975).
- [5] L. Salasnich, A. Parola, L. Reatto, Modulational instability and complex dynamics of confined matter-wave solitons, *Phys. Rev. Lett.* **91**, 080405 (2003).
- [6] F. Kh. Abdullaev, A. A. Abdumalikov, R. M. Galimzyanov, Modulational instability of matter waves under strong nonlinearity management, *Physica D* **238**, 1345 (2009).
- [7] I. A. Bhat, S. Sivaprakasam, and B. A. Malomed, Modulational instability and soliton generation in chiral Bose-Einstein condensates with zero-energy nonlinearity, *Phys. Rev. E* **103**, 032206 (2021).
- [8] B. B. Baizakov, A. Bouketir, S. M. Al-Marzoug, and H. Bahlouli, Effect of quintic nonlinearity on modulation instability in coupled nonlinear Schrödinger systems, *Nonlinear Sciences* **180**, 792, (2018).
- [9] V. E. Zakharov and A. A. Gelash, Nonlinear stage of modulation instability, *Phys. Rev. Lett.* **111**, 054101 (2013).
- [10] G. Vanderhaegen, C. Naveau, P. Szriftgiser, A. Kudlinski, M. Conforti, A. Mussot, M. Onorato, S. Trillo, A. Chabchoub, and N. Akhmediev, “Extra-ordinary” modulation instability in optics and hydrodynamics, *Proc. Natl. Acad. Sci.* **118**, e2019348118 (2021).
- [11] E. V. Goldstein, and P. Meystre, Quasiparticle instabilities in multicomponent atomic condensates, *Phys. Rev. A* **55**, 2935 (1997).
- [12] I. Kourakis, P. K. Shukla, M. Marklund, and L. Stenflo, Modulational instability criteria for two-component Bose-Einstein condensates, *Eur. Phys. J. B* **46**, 381 (2005).

- [13] T. Mithun, A. Maluckov, K. Kasamatsu, B. A. Malomed, and A. Khare, Modulational instability, intercomponent asymmetry, and formation of quantum droplets in one-dimensional binary Bose gases, *Symmetry* **12**, 174 (2020).
- [14] D. S. Petrov, Quantum mechanical stabilization of a collapsing Bose-Bose mixture, *Phys. Rev. Lett.* **115**, 155302 (2015).
- [15] D. S. Petrov and G. E. Astrakharchik, Ultradilute low-dimensional liquids, *Phys. Rev. Lett.* **117**, 100401 (2016).
- [16] G. E. Astrakharchik, B. A. Malomed, Dynamics of one-dimensional quantum droplets, *Phys. Rev. A* **98**, 013631 (2018).
- [17] Sh. R. Otajonov, E. N. Tsoy, and F. Kh. Abdullaev, Stationary and dynamical properties of one-dimensional quantum droplets, *Phys. Lett. A*, **383**, 125980 (2019).
- [18] Y. Li, Z. Chen, Z. Luo, C. Huang, H. Tan, W. Pang, and B. A. Malomed, Two-dimensional vortex quantum droplets, *Phys. Rev. A* **98**, 063602 (2018).
- [19] Sh. R. Otajonov, E. N. Tsoy, and F. Kh. Abdullaev, Variational approximation for two-dimensional quantum droplets, *Phys. Rev. E* **102**, 062217 (2020).
- [20] Y. V. Kartashov, B. A. Malomed, L. Tarruell, and L. Torner, Three-dimensional droplets of swirling superfluids, *Phys. Rev. A* **98**, 013612 (2018).
- [21] Sh. R. Otajonov, Quantum droplets in three-dimensional Bose–Einstein condensates, *J. Phys. B: At. Mol. Opt. Phys.* **55**, 085001 (2022).
- [22] N. B. Jørgensen, G. M. Bruun, and J. J. Arlt, Dilute fluid governed by quantum fluctuations, *Phys. Rev. Lett.* **121**, 173403 (2018).
- [23] I. Ferrier-Barbut, H. Kadau, M. Schmitt, M. Wenzel, and T. Pfau, Observation of quantum droplets in a strongly dipolar Bose Gas, *Phys. Rev. Lett.* **116**, 215301 (2016).
- [24] I. Ferrier-Barbut, M. Wenzel, M. Schmitt, F. Böttcher, and T. Pfau, Onset of a modulational instability in trapped dipolar Bose-Einstein condensates, *Phys. Rev. A* **97**, 011604 (2018).
- [25] C. R. Cabrera, L. Tanzi, J. Sanz, B. Naylor, P. Thomas, P. Cheiney, and L. Tarruell, Quantum liquid droplets in a mixture of Bose-Einstein condensates, *Science* **359**, 301 (2018).
- [26] T. G. Skov, M. G. Skou, N. B. Jørgensen, and J. J. Arlt, Observation of a Lee-Huang-Yang Fluid, *Phys. Rev. Lett.* **126**, 230404 (2021).
- [27] C. D’Errico, A. Burchianti, M. Prevedelli, L. Salasnich, F. Ancilotto, M. Modugno, F. Minardi, and C. Fort, Observation of quantum droplets in a heteronuclear bosonic mixture, *Phys. Rev.*

- Research **1**, 033155 (2019).
- [28] I. Ferrier-Barbut, Ultradilute quantum droplets, *Phys. Today* **72**, 46 (2019).
- [29] Z. H. Luo, W. Pang, B. Liu, Y. Y. Li, and B. A. Malomed, A new form of liquid matter: Quantum droplets, *Frontiers of Physics* **16**, 1 (2021).
- [30] E. Infeld, Quantitative theory of the Fermi-Pasta-Ulam recurrence in the nonlinear Schrödinger equation, *Phys. Rev. Lett.* **47**, 717 (1981).
- [31] M. Kramer, C. Tozzo, and F. Dalfovo, Parametric excitation of a Bose-Einstein condensate in a one-dimensional optical lattice, *Phys. Rev. A* **71**, 061602 (2005).
- [32] A. Görlitz, et al., Realization of Bose-Einstein condensates in lower dimensions, *Phys. Rev. Lett.* **87**, 130402 (2001).
- [33] C. Josserand and S. Rica, Coalescence and droplets in the subcritical nonlinear Schrödinger equation, *Phys. Rev. Lett.* **78**, 1215 (1997).